Analysis of Electrocardiographic Patterns for Epileptic Seizure Prediction

Francisco Sargo[1]

Abstract— **The gold standard for the diagnosis, and automatic detection and prediction of epileptic seizures is based on data gathered by long term EEG. This modality requires highly intrusive hardware, with limiting aspects such the great number of electrodes placed on the subject's scalp. For this reason, it is typically performed in clinical settings, and it is often seen as too intrusive by the users.**

There is therefore, a need for an ambulatory and comfortable monitoring application to control seizures, consisting of a seizure prediction method such as single Lead ECG acquisition, which can be performed with a more comfortable hardware, and which can easily be integrated into a wearable system.

The purpose of this work is to evaluate some of the required methodologies for the development of a seizure prediction algorithm based on ECG data in signals acquired by a Lead-I setup. It involves the application of noise and baseline wander removal techniques, detection of fiducial points and robust computation of morphological and rhythmical features. The work culminates in the attempt to distinguish between inter-ictal and pre-ictal moments, with the use of supervised learning classifiers such as Support Vector Machines (SVM), K-Nearest Neighbours (KNN), and Gaussian Naive Bayes (GaussNB). This study comprises N=44 seizures acquired from 5 patients admitted at SMH in Lisbon.

I. Motivation

Epilepsy is an important cause of disability and mortality, affecting almost 70 million people worldwide and with a median incidence of 0.0005% per year and more common in children than adults [1]. A person with epilepsy would be affected by abnormal brain activity, causing seizures that may vary in degree from hardly noticeable, to severe, threatening their own life and possibly the life of others.

Common symptoms of these seizures are disturbance of consciousness and sudden loss of motor control, which typically occur without any type of warning. Thus, the ability to predict epileptic seizures, can reduce patient anxiety and alleviate the immeasurable constraints and secondary behavioral disturbances posed by this disorder.

Another key advantage to predict an incoming seizure is the widening of therapeutic options, meaning that long-term treatment with anti-epileptic drugs, with cognitive or other neurological side effects, could be reduced to a targeted and short-acting intervention, thus improving quality of life and safety [2].

The gold standard in the detection, diagnosis and automatic prediction of epileptic seizures is prolonged Video-Electroencephalograhy (vEEG). This modality not only requires intrusive hardware, like great number of electrodes and complex acquisition systems, but relies also on constant monitoring for integrity and safety of the devices, besides being extremely uncomfortable and unsightly. For these reasons it is typically performed in a clinical setting, and it is not suitable for use in the daily life activities. Even though treatment through anti-epileptics has success with most patients, a significant portion still experiences attacks [3], reinforcing the need for ambulatory monitoring mechanisms to predict seizures onset that should minimally affect comfort.

The Electrocardiography (ECG) signal is a notable example of easily acquired physiological information, which according to recent research may provide valuable insights in seizure prediction [4], [5], [6]. Single-lead ECG data acquisition involves only 2 to 3 minimally intrusive surface electrodes resorting to simple, miniaturized and inexpensive electronics, which means the setup can be implemented in highly comfortable, concealable and cost-effective hardware.

The task of automatic seizure prediction from biosignals is an extensively studied subject in the literature. The basic structure of the methodology, common to all publicly available methods is the extraction of patterns from contiguous acquisitions of from signal records that can manifest some indicative epiliptogenic variations before the seizure onset. A logical conceptual subdivision of the types of patterns is to group them into either morphological, concerning the morphology of the cyclic heart wave, or as rhythmic pattern capturing the rhythm of the cyclic heart beat, which is commonly described as Heart Rate (HR).

II. Theory

A. The heart-beat waveform

A measurement through time of the electric potential difference on the surface of the skin, captures the electrical field fluctuations caused by the heart electrodynamics. This quasi-periodic, non-stationary and non-linear signal is the ECG.

The quasi-periodicity of this time series allows for the identification of a common ECG complex with 5 basic components as depicted in Figure 1. Although there is a great deal of variation in the morphology of the ECG-waveform across different patients, they are often identifiable as P, Q, R, S and T waves, as illustrated in Figure 1.

The heart cycle begins with the impulse generation by the Sino-Artrial (SA) node. As the mass of depolarized tissue is very small, this initial disturbance is hardly detected by the surface electrodes. But as more and more tissue depolarizes, the difference of potential becomes noticeable.

[1]Técnico Lisboa francisco.simao.sargo@tecnico.ulisboa.pt

As the depolarization spreads from the SA node through to the atria, the first deflection, the P-wave occurs in the signal. The ending of such deflection marks the complete depolarization of the atria and their subsequent contraction. The deflection is succeeded by a return to baseline, which corresponds to a period where action potentials spread to atrioventricular node and bundle of His. Next, 160 ms after the beginning of the heart cycle, the right and left ventricles begin to depolarize, marking the event measured in the QRS complex (QRS). As this occurs simultaneously with the repolarization of the atria and since the repolarization mass is considerably inferior to the much larger ventricular depolarization mass, the effect is masked by the QRS, and it is not usually detected by the ECG.

As the depolarization spreads from the SA node through to the atria, the first deflection, the P-wave occurs in the signal. The ending of such deflection marks the complete depolarization of the atria and their subsequent contraction. The deflection is succeeded by a return to baseline, which corresponds to a period where action potentials spread to atrioventricular node and bundle of His. Next, 160 ms after the beginning of the heart cycle, the right and left ventricles begin to depolarize, marking the event measured in the QRS. As this occurs simultaneously with the repolarization of the atria and since the repolarization mass is considerably inferior to the much larger ventricular depolarization mass, the effect is masked by the QRS, and it is not usually detected by the ECG.

The ensuing repolarization of the ventricles after contraction, causes the last normally detected deflection in the ECG beat, which is followed by the P-wave of the next cardiac cycle. It is very important to note that deflections in the ECG wave do not correspond to the actual contractions from the heart, which although being the result of the initial depolarization, occur in a longer time-scale.

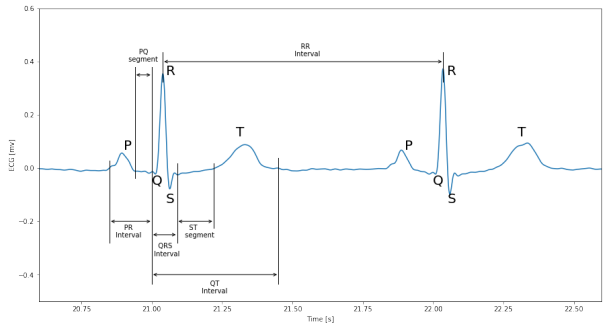

Fig. 1: Depiction of the basic structure of an ECG waveform, a quasi-periodic of the variation of the surface potential in volts over time. It outlines the existence of the 5 major complexes: the P, Q, R, S, and T waves. Adapted from [7].

B. A Primer on Epilepsy

A definition of epilepsy, introduced by the International League Against Epilepsy (ILAE) [8], defines the pathology as a disorder of the central nervous system, which manifests itself mainly in the form of transient, recurrent and unprovoked seizures resulting from an abnormal, excessive and hyper-synchronous discharge of a population of cortical neurons, so called *epileptic seizures*.

III. The Cardiovascular properties of epilepsy

A. Underlying mechanisms

As of now, there is little understanding about the mechanisms behind cardiovascular changes in epilepsy [9]. Despite this, a growing number of evidence supports the involvement of cortical structures that constitute the CAN (including the amygdala and the insular cortex), and the involvement of adaptive cardiovascular reflexes triggered by ictal manifestations [10]. As of now, there is little understanding about the mechanisms behind cardiovascular changes.

A well-known dynamic of the ANS is that parasympathetic and sympathetic systems act in concerted manner to maintain homeostasis and regulate key visceral functions such as the HR. In particular, the anterior cingulate, insular, posterior orbito-frontal, and the pre-frontal cortices play key roles in influencing the ANS, at the cortical level along with the amygdala and hypothalamus, as depicted in Figure 2.

A proposed explanation found in [11] is that, in patients suffering with epilepsy, ictal discharges that occur in or propagate to these structures which leads to increased sympathetic outflows, impacting autonomic function. In fact, research involving experimental stimulation of different neural structures suggests that the propagation of epileptic discharges to the right insular cortex is a primary driver of sympathetic-parasympathetic changes that influence HR.

A common effect is Ictal Tachicardia (IT), but parasympathetic responses such as decrease in HR can also occur, if the ictal discharges propagate to cortical regions governing depressor responses. This activation of central autonomic nervous system is thought to be responsible for the acute cardiac changes.

Peripheral effects combined with autonomic alterations triggered by seizures may explain some of the morphologic ictal ECG changes. As an example, the ictal ST elevation/-depression and T-wave inversion most likely reflect cardiac ischemia due to a mismatch between myocardial oxygen demand and supply in IT. This situation may be amplified further when IT is associated with hypoxia.

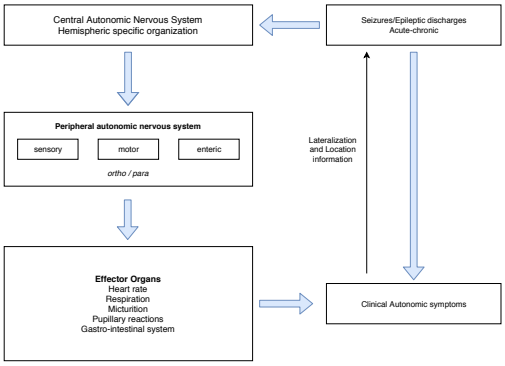

Fig. 2: Origin of autonomic symptoms in epilepsy (adapted from [11]).

B. Basis for ECG-based automatic epileptic seizure prediction

As the available literature makes a clear explanation of the influence exerted on cardiac activity by the hyper-synchronous firing of cortical neurons in the epileptic seizure onset, there is little doubt whether ECG could be a successful vector of information to perform seizure prediction.

The subjective evaluation of bio-signals, such as Electroencephalography (EEG) and ECG, makes automatically extracted parameters (computer-based) highly useful for diagnostics. Moreover, due to the difficulty of visual investigation of multi-parametric recordings (in this case time-synchronous EEG and ECG) and in combination with the progress of signal processing and pattern recognition methodologies, many approaches for automatic detection of seizures have been proposed in the literature.

Another clear advantage is that ECG acquisition can be minimally invasive and easily adaptable to simple wearable devices, a portable, highly flexible and robust ECG-based predictive system of epileptic seizures could ideally be coupled with a reactive seizure avoidance tactic forming a so-called closed-loop seizure system.

IV. Methodology

A. General Overview of the Methodology

The methodology proposed in this work is depicted in the following schematic:

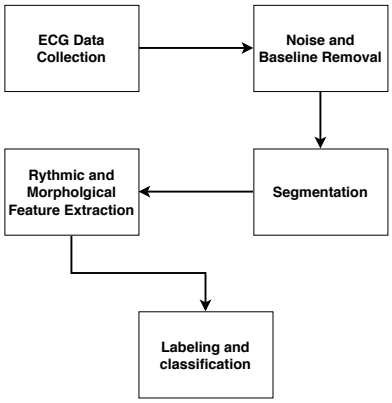

Fig. 3: Depiction of the sequence of steps employed by the Hamilton Algorithm.

The methodology pipeline starts with the collection of the ECG data from the Santa Maria's Hospital (SMH) servers, comprehending extraction and conversion of the raw files present in the hospital's system, creation of the appropriate annotations for the data, primary division of the contiguous data into fixed time-frames of analysis called 'seizure sessions' and building of the final database with every seizure session.

This is followed by a step of filtering to reduce the baseline wander of the signal and the corruption by noise and artifacts, important steps for a successful feature extraction. The process of signal segmentation is next, with the detection of the R-peaks (RP) by means of the algorithm proposed by [12]. Based on this segmentation, the Heart Rate Variability (HRV) signal can be derived and heart-beat wave templates from the ECG extracted.

From the HRV signal and the series of templates,the feature extraction can be done resorting to a moving window of 5 minutes with a 98 % overlap, to compute the time series used for this analysis. The previous computation is followed by a labeling of the samples into pre-ictal and inter-ictal, which groups data from two different time-zones of the acquisition, which are in fact labels relevant to the production of an alarm or prediction. On these computed profiles, and the labeled samples, supervised binary classification algorithms can be trained and tested to evaluate the possibility to distinguish and model the separation of the two classes.

B. Dataset restructuring

To create a common time frame of analysis for each seizure, it was necessary to divide the continuous ECG time-series into fixed time frames of analysis called 'seizure sessions'. These seizure sessions were extracted having as a reference the time instant of the EEG onset. The rationale for this division, besides the standardization of the temporal analysis across seizures, was also to expedite and ease the implementation of the processing tools for the whole dataset. Having multiple blocks of fixed duration with respect to the seizure onsets allowed for a more 'modular' and 'segmented' database, with a single unitary dataset referring to only one seizure holding either the raw signals from the acquisition or even the multi-dimensional extracted feature-space relative to that seizure. Another advantage of such procedure is the possibility to easily parallelize the execution of the data analysis pipeline, since each seizure can be processed in parallel to each other, thus increasing the speed of the implementation.

From the raw data, the selection of the suitable seizure events, and valid time instants for analysis was performed having in consideration a number of requirements:

- A maximum time interval of 2 hours preceding the onset was considered for each seizure;
- Events with onset separated from the previous one by a duration of less than 1h and 30 minutes were discarded;
- Data points for a particular seizure onset within a 30 minute length window with respect to the previous onset were discarded.

The outlined requirements are a compromise between the amount of gathered data from the hospital, the necessity to have an expressive segment of samples preceding each onset and to guarantee a considerable separation between different onsets.

A problem to overcome in the process of building these seizure sessions, was the occurrence of data drop-outs between the acquisition chunks saved by the Neurofax system. As said before the Neurofax system creates regular chunks with a maximum fixed duration of 2 hours, leading to drop-outs of the acquisition in-between the chunks. Also, due to the unpredictable and often violent eruptions of the motor manifestations from the epileptic patient, there is also

a number of intervals within some chunks with no data acquisition.

The creation of the session generates a continuous time frame of analysis, including ECG and missing data. These periods without any acquisition are dealt with in the posterior stages of feature extraction by rolling window.

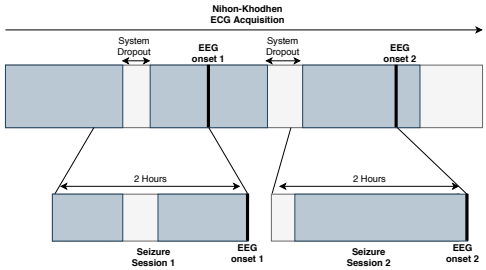

Fig. 4: Schematic illustrating the creation of fixed duration time frames of analysis called seizure sessions from the raw, continuous data.

C. ECG heartbeat waveform segmentation

The detection of fiducial points in ECG was employed using the algorithm proposed by [12], in which the main steps are outlined in the schematic shown in Figure 5.

The fiducial point of choice in this work is the R-peak, which stands as the highest peak in the QRS. The method relies on an initial filtering stage of the ECG data, with the sequential application of a 4^th order low pass and high pass filters, with a resultant passing band between 6 and 18Hz. This modal filtering technique targets the removal of high frequency components that may misguide the detection of the RP.

A moving average filter with a width of 80 milliseconds, is then computed on the absolute value of the first derivative of the filtered signal. This pipeline of linear operations ensures a final signal that contains small "lumps"in the place of the QRS. Afterwards, in a effort to discriminate between true RP and outliers, a set of simple detection rules is used:

1) Ignore all peaks that precede or follow larger peaks by less than 200 milliseconds;
2) If a peak is detected, check to see whether the raw signal contained both positive and negative slopes. If not, the peak represents a baseline shift;
3) If the peak occurred within 360 milliseconds of a previous detection check to see if the maximum derivative in the raw signal was at least half the maximum derivative of the previous detection. If not, the peak is assumed to be a T-wave.
4) If the peak is larger than the detection threshold, select a RP otherwise consider it noise;
5) If no RP has been detected within 1.5 RRI intervals, there was a peak larger than half the detection threshold, and the peak followed the preceding detection by at least 360 milliseconds, classify that peak as a RP.

The detection threshold used in steps 4 and 5 is computed based on estimates of the RP and noise peak heights. If a peak is indeed part of a QRS, it is added to a buffer containing the eight most recent RP. When a peak is not classified as a RP, it is added to a buffer containing the eight most recent non-RP. The detection threshold is set between the mean or median of the noise peak, and QRS peak buffers according to the equation:

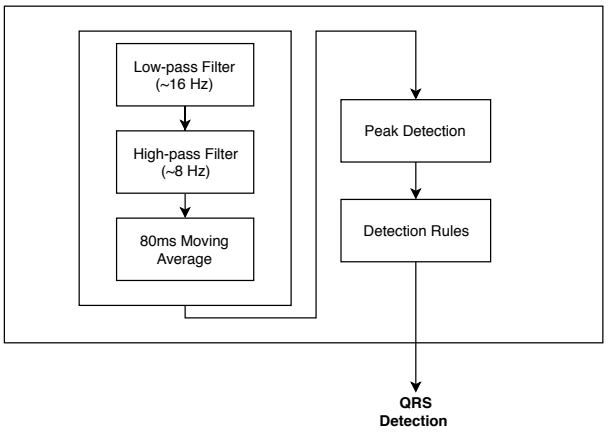

Fig. 5: Depiction of the sequence of steps employed by the Hamilton Algorithm.

$$DT = ANP + TH(AqrsP - ANP) \quad (1)$$

with, $DT - DetectionThreshold$, $ANP - AvergeNoisePeak$, and $AqrsP - AverageQRSPeak$.

The Python implementation of the algorithm used in this work is contained within the open-source *Biosppy* package. From the QRS the time instants of the RP are kept and the detection of the RP is then used to compute the HRV signal and to extract different templates from the ECG signal.

D. RR tachogram computation

Following previous segmentation of the data with RP detection, the R-to-R signal (RR) was computed by the time differences between adjacent RP. The easy derivation of the signal has popularized its use in cardiac analysis and it is now a wide-spread metric in several devices in the market for different purposes [13].

The acquisition of ECG data at a sampling frequency of $1000Hz (> 500Hz)$ was ideal to engage in HRV analysis, since this sampling rate is well above the lower bound value of $500Hz$ bellow which the error rate of RP detection in patients with low HR is highly significant.

E. Outlier removal

A common problem in the analysis of ECG signals is the occurrence of outliers. In a continuous ECG time series, the HRV can be defined as the so-called N-to-N intrevals (NN) intervals, that is, all intervals between adjacent QRS complexes resulting from sinus node depolarization. This means that the computation of the time series must be robust to the occurrences of RP misdetections.

As explicited in the previous subsection, the method by Hamilton already employs a set a threshold-based rules to

minimize the occurrence of misdetected peaks. Yet, in the presence of heavily corrupted signals (for example with Electromyography (EMG) artifacts) there is so much this set of rules can do, and often the detector still produces misclassifications. In that spirit, a posterior step of outlier removal is an appropriate solution to deal with this kind of unwanted signal. This work relies on the method and implementation developed by Miguel Martinho at IT Lisbon, which detects outliers based on an time-wise adaptive threshold that takes into account not only the HRV signal, but also the amplitudes of the RP.

After an initialization of the analysis in the first detected RP, the algorithm evaluates the next RP to decide whether or not it is valid, based on the previous peaks. It takes into account if the peak in the analysis results in the computation of unphisiological values of HRV, (Higher than 180 Beats per minute (bpm) and lower than 80 bpm), and decides if the amplitude of such beat is above a percentage of the mean amplitude of the previous beats or the resulting HRV is above a percentage of the mean HRV.

The flowchart of the process is shown in Figure 6.

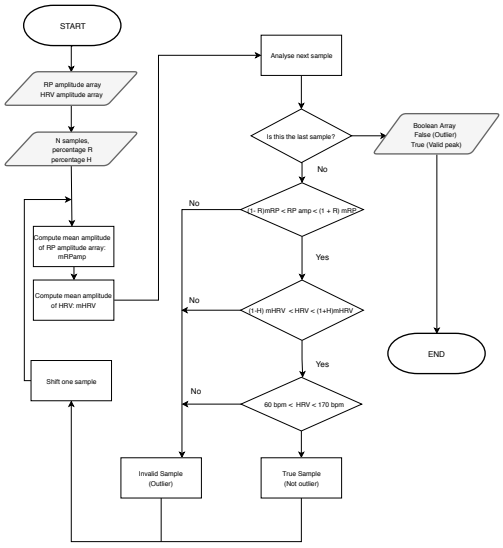

Fig. 6: Flow-chart illustrating the process of outlier removal, as developed by Miguel Martinho.

F. Rhythmic Patterns

From a series of instantaneous heart rate measurements, the RR signal, a number of metrics can be extracted. The multi-dimensional array of such metrics can be conceptualized as rhythmic patterns of the ECG, since they are an indicator of the rhythm of the heart-cycle and can be derived from ECG signal.

G. Statistical HRV Features

A common framework of analysis of the HRV is the statistical description of the signal in particular time segments, usually framed as windows. These may be subdivided into two classes, (a) those derived from direct measurements of the NN intervals or instantaneous heart rate, and (b) those derived from the differences between NN intervals.

Some examples of (a) can be:

- **MeanNN**: The mean value of the NN in a given window;
- **SDNN**: The standard deviation of the NN in a given window;

The Standard Deviation of Normal-to-Normal intrevals (SDNN) being the square-root of variance, which is mathematically equal to total power of spectral analysis, reflects all the cyclic components responsible for variability in the period of the signal. In many studies, SDNN is calculated over a 24-h period and thus encompasses both short-term high frequency variations, as well as the lowest frequency components seen in a 24-h period.

And in the (b) category, some examples of features are:

- **RMSSD**: Root Mean Square of Successive Differences
- **NN50**: Number of pairs of adjacent NN intervals differing by more than 50 ms
- **pNN50**: Proportion of pairs of adjacent NN intervals differing by more than 50 ms

These metrics estimate high-frequency variations of the signal and thus are highly correlated.

H. Spectral HRV Features

The power spectral analysis of heart rate fluctuations to quantitatively evaluate beat-to-beat cardiovascular control is of major importance in the evaluation of the autonomic background of NN interval fluctuations. Three main spectral components are distinguished in a spectrum calculated from short-term recordings of 2 to 5 min, which are the Very Low Frequency (VLF), the Low Frequency (LF) and the High Frequency (HF) bands.

- **VLF**: Power expressed by the range of frequencies between $0.003Hz - 0.04Hz$.
- **LF**: Power expressed by the range of frequencies between $0.04Hz - 0.15Hz$
- **HF**: Power expressed by the range of frequencies between $0.15Hz - 0.4Hz$

There are however some caveats with the physiological explanation of the VLF component, being much less defined since the existence of any connection to a physiological mechanism is questionable. The ratio between the two frequency bands can be defined as the Low Frequency/High Frequency ratio (LF/HF), and expresses the balance between the sympathetic nervous system activity and the parasympathetic nervous system activity [13].

Figure 7 highlights an important problem with these metrics. The evaluation of the HRV spectrum for the same subject in different types of physical activity, at rest and with a head tilt, creates two different Power Spectral Density (PSD) profiles, with different contributions from the frequency bands and different values of total power. Although the relative contribution of the LF band increases with the head tilt, the absolute value of power remains the same, by virtue of the overall decrease in total variance.

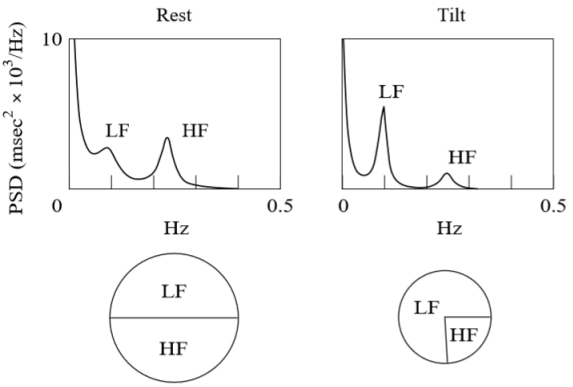

Fig. 7: Depiction of the HRV spectrum on two different signals, acquired at different periods of a patient's activity, (left) at rest and (right) with head tilt. It is possible to note that with the tilt the LF component becomes dominant but, as total variance is reduced, the absolute power of LF appears unchanged compared to rest. It can also be noted that the different power distribution of both spectrums highlights different contributions of both components of the autonomic nervous system, adapted from [13].

In order to capture the relative change it is possible to compute the normalized metrics, which can be defined according to [5] as the ratio between the absolute power of the bands and the total power, described as Normalized Low Frequency (LFnu), Normalized High Frequency (HFnu).

The HRV signal is derived from the RP of the ECG signal, and the sampling of such derived series is uneven, which means the timing of the RP is dependent on heart rate. This poses a difficult problem to the spectral analysis, since methods based on the Fast Fourrier Transform (FFT) require regularly sampled signals.

The typical proposed solution is to resample the signal into a regularly sampled signal by means of interpolation. The ideal choice is cubic-spline interpolation, since it allows for a smooth estimate of the signal to a fixed a pre-determined sampling rate [5].

A common value for the sampling frequency is 1 Hz, as it is well over the Nyquist frequency of the HRV signal, for which an example of the spectrum can be found on Figure 7. The computation of the power spectral density of the then resampled signal can be made resorting to different methods.

The classical periodogram is one non-parametric possibility suffering from severe drawbacks, since the result of the estimation can be highly inaccurate, given the methods employed in the signal. Another way to evaluate the power spectral density of the signal, is to use the Lomb-Scargle periodogram [14], which contrary to the classical periodogram estimates the PSD based on a least-squares regression, thus not requiring the extra step of resampling [15]. Non-parametric methods are usually more efficient, given the simplicity of the employed algorithms FFT and high-processing speed. An example of a parametric method is to use an auto-regressive model. Another alternative, is to use a non-parametric method. The auto-regressive model allows for a smoother estimation, provided the right order of the model is chosen, which according to [16] can be no less than 16.

I. Morphological Features

1) Heart-beat waveform: To consider potential morphological determinants involved in epiliptogenesis, a common pre-requisite is to extract the heartbeat waveform the ECG based on a particular set of fiducial points. The extraction of i-th heart wave segment b is essentially a segmentation of the data points from a predefined interval, with respect to the detection of the i-th RP according to Equation (3) and as depicted in Figure 8:

$$b_i(t) = ECG(t),\ RP(i) + N_1 < t < RP(i) + N_2, \quad i = 0, 1, 2, 3, 4, 5... \tag{2}$$

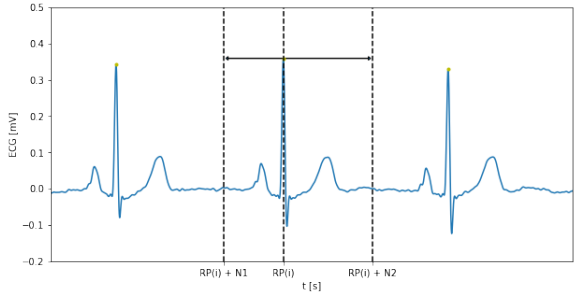

Fig. 8: Illustration of the process for fixed length heart-wave extraction from the ECG based on detection of RP.

J. Distance between heart-waves

The extraction of morphological patterns of the ECG can be done with the computation of a similarity coefficient between heart-wave b_i and b_l. The most basic measurement is the euclidean distance between the two templates. Another more useful notion of distance is the pearson correlation coefficient ρ, which stands as a covariance of the two templates b_i and b_l, divided by the product of their standard deviations, formally:

$$\rho_{b_i,b_l} = \frac{cov(b_i, b_l)}{\sigma_{b_i}\sigma_{b_l}} \tag{3}$$

Varying from 1 to -1, the metric is robust to linear changes in the heart-waves, and thus it is particularly sensible to non-linear differences between the two.

K. Extraction of Statistical HRV Features

However, It is important to note that the rhythmic features are heavily specific to each patient, each emotional state and dependent on the circadian rhythm, which means that the absolute values of such time profiles may be difficult to compare across seizures and patients.

One possible work-around to this problem, and one tested in this work was to consider a 10 minute length initial

window defined as the first 10 minutes of the seizure session to serve as control, and instead of the calculation of the absolute values for each feature, the computation of the ratio between the metric computed on a posterior 5 minute length window and the metric computed on the control window.

L. Classification of Different Time-zones Within a Seizure Occurrence

A simple and straightforward method to discern the possibility of a pre-ictal state within the pattern time-series of a seizure session (a state that could serve as a basis for an alarm), is to arbitrarily label samples in two regions of the session as belonging to two different classes. A possible labeling criteria is to say that, for each seizure, the samples within 30 minutes before the EEG-onset belong to pre-ictal class (red), and the points lying within the time period from the beginning of the seizure session with a duration of 30 minutes belong to inter-ictal class (red) as depicted in Figure 9. The points in-between the time-periods belong to an unspecific non-labeled group, that is points that do not belong to any class.

The problem of modeling the separation between both classes and to automatically classify unsees samples is a typical binary supervised learning problem.

This particular labeling scheme allows for the classifiers to learn from samples from two different time-periods considerably far apart from each other within the seizure session, likely maximizing the separation between pattern samples from different classes, which in turn will result in a more optimized classification task.

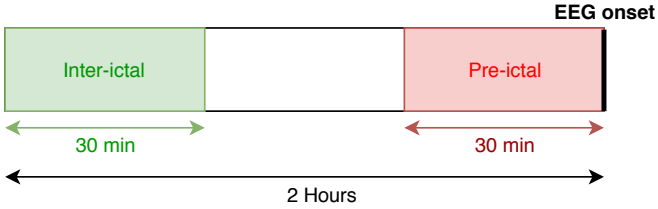

Fig. 9: Figure depicting the labeling criteria of the data within each seizure occurrence.

M. Sample-by-sample classification

Typical metrics to assess classification performance are precision (positive predictive value) and recall (sensitivity), which can be expressed as functions of true positives (TP), false positives (FP), true negatives (TN) and false negatives (FN):

$$Precision = \frac{TP}{TP + FP} \tag{4}$$

$$Recall = \frac{TP}{TP + FN} \tag{5}$$

A given algorithm can be used to fit a specific model based on the maximization of one of these scores. Yet, for a particular choice of labeling criteria, the resulting datasets can be heavily impacted by class imbalance (much more inter-ictal data points). For this reason, care must be taken on the choice of the metric to maximize, as for example maximizing accuracy could simply result in a decision function favoring the over-represented class.

A better solution is to optimize for recall or precision. Ideally a ponderation of both. A single metric comprising both these dimensions is the F-score, which is the harmonic mean of the scores:

$$F1 = \frac{2.TP}{2.TP + FP + FN} \tag{6}$$

N. Leave-one-seizure-out nested cross-validation

In order to get a good sense of the generalization performance, the models are trained based on leave-one-seizure-out (LOSO) N-fold nested cross-validation scheme, as represented by Figure 10. Following this paradigm, each seizure of the N total in the dataset is chosen to evaluate the predictive performance on unseen seizures, and the remaining N-1 seizures are left for training. The training set is further subdivided, again leaving one seizure for validation and N - 2 for the training of the model with a particular set of hyper-parameters. Each seizure is chosen once to serve as validation. In this nested fold, the algorithms are trained with different sets of hyper-parameters, and the set producing the highest mean validation score is chosen, the set of hyper-parameters is then used to retrain the classifier on the training set. For each seizure an optimized model is trained on the data from other seizures.

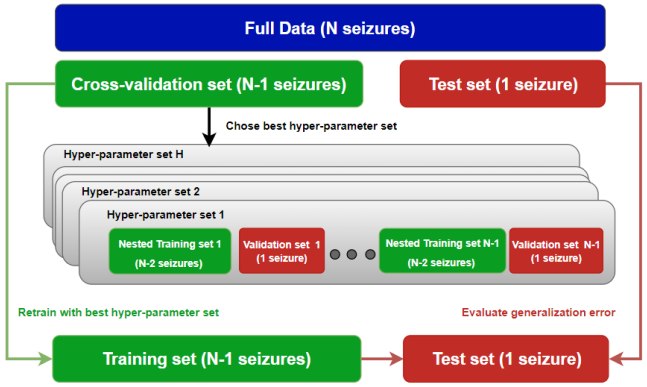

Fig. 10: Nested Cross Validation Scheme.

As referenced in [17] using different sub-sets of the data to optimize a given classifier's hyper-parameters than the one used to evaluate the classifier's performance is important to prevent information leakage from training set and thus overfitting.

O. Features Categorization

In order to succinctly evaluate the results from each type of feature, appropriate codes must be given to the features. The computed features can be divided into 2 main groups: feature-set M and feature-set R.

Feature-set M, comprises the morphological features computed from the extracted fixed length heartbeat waveforms, based on the previous RP fiducial point detection. Metrics referring to the Euclidean distance belong to the feature group $M.1$, metrics referring to the Pearson correlation coefficient are grouped under the group M.2, subdividing each group in (a) for metrics computed on the beat and (b) for metrics computed on the QRS.

Feature-set R, comprises the features related to heart-rate variability, which entails also the ratios between statistical computations on the NN intervals such as the Mean Normal-to-Normal intervals (meanNN) and the SDNN, belonging to feature group R.1, together with spectral considerations of the epochs, which belong to feature group R.2.

P. Classifiers

A number of supervised classification algorithms were used in this work:

- **KNN (K-Nearest Neighbours)**
- **SVC (Soft-Margin Support Vector Machines with radial basis kernel)**
- **GaussNB (Gaussian Naive Bayes)**

V. Results and Discussion

A list of patients made accessible to this work is described in I. Each patient information such as age, gender and last name was retrieved from the written paper notebooks produced by the unit's staff. These characteristics could then be introduced in the system to access the data.

TABLE I: General description of the data set

	Patient 3	Patient 5	Patient 8	Patient 10	Patient 13
Age	30	42	31	28	43
Gender	f	f	m	m	f

Table II presents the events considered for analysis in this work. Each entry corresponds to the description of a seizure block, a common time-frame of analysis, which serves as session or as a series of data containing only one seizure. It also holds a description of seizure type and location. The information in the table concerns information present in the written reports by the EEG specialists at SMH, and describes for each event the type of seizure following the ILAE convention. This represents a reduced dataset since it only presents the seizures that respect the segmentation rules described before.

Given the discussed cross-validation scheme, the capability of the classifier to distinguish a pre-ictal zone from each seizure session (each one belongig to the test set) can be measured by the F1-score.

The folowing tables hold the mean and standard deviation of the F1-score across a number of different seizures.

Tables III and IV present the statistics across seizures of a particular hemisphere, using (respectively) the K-Nearest Neighbours classifier and the Gaussian Naive-Bayes Classifier.

TABLE II: Description of the Events in the dataset

Patient ID	**Seizure ID**	Type of Seizure	Location
3	**0**	G - A - M	L-R (F, T)
	1	F - NA - M	L (F, T)
	2	F - A - M	L (F, T)
5	**0**	F,SG - NA - M	L (C, FC)
	1	F - NA - NM	L (C, FC)
	2	F,SG - NA - M	L (C, FC)
	3	F,SG - NA - M	L (C, FC)
	4	F,SG - NA - M	L (C, FC)
	6	F,SG - NA - M	L (C, FC)
8	**0**	F - A - NM	R (FT, T)
	1	F - NA - NM	R (FT, T)
	2	F - A - NM	R (FT, T)
	3	F - NA - M	R (T)
	4	F - A - M	R (T)
	8	F - NA - Mr	R (T, TP)
	9	G - NA - M	R (T, P, F)
	10	F,SG - A - M	R (T, P, F)
10	**0**	F,SG - A - M	L (F, FT, F, FC)
	1	F,SG - NA - M	L (FT, T)
	2	F,SG - NA - M	L (F, FT)
	3	F,SG - NA - M	F (F, FT)
13	**0**	F - NA - NM	R (P, O, PO)
	1	F,SG - A - NM	R (P, O, PO)
	3	F,SG - A - NM	R (P, O, PO)
	4	F,SG - A - M	R (P, O, PO)

Event classification: G-Generalized, F-Focal, A-Aware, NA-Not Aware, M-Motor, NM-Non Motor
Event Location: R-Right Hemisphere, L-Left Hemisphere, F-Frontal , FT-Fronto-temporal,

Tables V, VI, VII, present the results for the statistics across seizures of a single patient, that is patient-specific classification, using (respectively) the K-Nearest Neighbours classifier and the Gaussian Naive-Bayes.

Theoretically, as discussed in section III-A, a primal indicator of pre-ictal change is the IT, a manifestation which would be reflected on the rhythmical features R1.a and R.2. By evaluating the results of the classifier trained on seizures from different brain hemispheres one can percieve that the K-nearest Neighbour classifier produces the Gaussian Naive Bayes produces the best results. Considering the Patient-specific classification results, and evaluating the performance of different feature groups in the classification task, one can state that across different classifiers, the best results are consistently produced by the same feature groups, with the few exceptions. This suggests that irresceptively of the trained model, the classifier can perform best on the same characteristics of the patient's signals.

Yet there is no clear distinction on which feature group performs the best irrespective of the Patient. For different Patients the best feature group varies, which indicates that for some patients, for example Patient 3, 5 and 8 the best feature group is a morphological feature group, suggesting that there is a more pronounced modification in morphology for these patients which is indicative of the the pre-ictal sample. In other patients the best performance is brought about by ryhtmic feature groups, which suggests pre-ictal rythmic alterations.

The best results in terms of best patient are also consistent

across classifiers: Patient 13 and 8 produce the best overall F1-scores. This is not unexpected, since these patients have the best quality data (that is less drop-outs) and the highest number of seizures (in the case of Patient 8).

Comparing the different classifiers one can notice that there is little difference between the 3.

It is important to note the high values of standard-deviation of the metric, which indicates that there is high variation of the score across seizures from the patient (in the case of patient-specific classification) or across seizures from a particular location. This value becomes much smaller in patients with a greater number of seizures or in greater groups of seizures.

TABLE III: F1-score Patient-specific classification results

Model	Key	Value	Feature Group	mean	std
KNN	location	L	M.1.a	0.334950	0.210431
			M.1.b	0.371868	0.210121
			M.2.a	0.643948	0.169123
			M.2.b	**0.665838**	0.222038
			R.1.a	0.000000	0.000000
			R.2	0.619446	0.172970
		R	M.1.a	0.446437	0.318097
			M.1.b	0.503321	0.186562
			M.2.a	0.480780	0.292740
			M.2.b	0.491935	0.288117
			R.1.a	**0.506409**	0.258086
			R.2	0.470361	0.260333

L - Left Hemisphere, R - Right Hemisphere.

TABLE IV: F1-score Patient-specific classification results

Model			Feature Group	mean	std
GaussNB	location	L	M.1.a	0.184852	0.163771
			M.1.b	0.255394	0.201751
			M.2.a	0.433849	0.251440
			M.2.b	0.456123	0.306586
			R.1.a	0.000000	0.000000
			R.2	**0.612912**	0.226102
		R	M.1.a	0.480343	0.325116
			M.1.b	0.540186	0.330798
			M.2.a	**0.724663**	0.202207
			M.2.b	0.593247	0.260356
			R.1.a	0.630730	0.245800
			R.2	0.596672	0.327202

L - Left Hemisphere, R - Right Hemisphere.

VI. Conclusions

Despite the unclear results, the use of patterns from ECG signals is promising. The fundamental steps of implementation were employed sucessfully to produce the preceding

TABLE V: F1-score Patient-specific classification results

Model	Patient ID	Feature Group	mean	std
GaussNB	3	M.1.a	0.353563	0.324501
		M.1.b	0.267756	0.332114
		M.2.a	0.207458	0.181678
		M.2.b	0.419585	0.307479
		R.1.a	**0.587264**	0.151001
		R.2	0.505716	0.028552
	5	**M.1.a**	**0.547318**	0.474455
		M.1.b	0.058043	0.100534
		M.2.a	0.186603	0.323206
		M.2.b	0.297862	0.285670
		R.1.a	0.410145	0.410823
		R.2	0.441436	0.382296
	8	M.1.a	0.656926	0.332435
		M.1.b	**0.740897**	0.228679
		M.2.a	0.619074	0.324936
		M.2.b	0.537145	0.277085
		R.1.a	0.581088	0.214933
		R.2	0.057063	0.098927
	10	M.1.a	0.261559	0.453033
		M.1.b	0.263298	0.456045
		M.2.a	**0.414241**	0.396358
		M.2.b	0.267930	0.464068
		R.1.a	0.359520	0.311817
		R.2	0.403191	0.356979
	13	M.1.a	0.676272	0.135595
		M.1.b	0.656394	0.054692
		M.2.a	0.661765	0.478337
		M.2.b	**0.684332**	0.446422
		R.1.a	0.672452	0.126219
		R.2	0.666935	0.122772

TABLE VI: F1-score Patient-specific classification results for the KNN classifier

Model	Patient ID	Feature Group	mean	std
KNN	3	**M.1.a**	**0.531194**	0.241979
		M.1.b	0.287303	0.250320
		M.2.a	0.179850	0.175632
		M.2.b	0.130800	0.111028
		R.1.a	0.397879	0.247313
		R.2	0.386656	0.126639
	5	**M.1.a**	**0.473298**	0.418639
		M.1.b	0.451321	0.468124
		M.2.a	0.331064	0.335386
		M.2.b	0.424336	0.461310
		R.1.a	0.289989	0.252221
		R.2	0.457251	0.397088
	8	**M.1.a**	**0.714236**	0.188940
		M.1.b	0.692189	0.242288
		M.2.a	0.666027	0.167079
		M.2.b	0.618642	0.177675
		R.1.a	0.515765	0.203572
		R.2	0.379306	0.128348
	10	M.1.a	0.274637	0.441271
		M.1.b	0.256954	0.445057
		M.2.a	0.370516	0.341329
		M.2.b	0.264706	0.458484
		R.1.a	0.338130	0.293325
		R.2	**0.408131**	0.353475
	13	M.1.a	0.667472	0.022325
		M.1.b	0.530074	0.037077
		M.2.a	**0.674886**	0.250036
		M.2.b	0.538327	0.485116
		R.1.a	0.483854	0.194945
		R.2	0.542955	0.056255

TABLE VII: F1-score Patient-specific classification results for the SVC classifier

Model	Patient ID	Feature Group	mean	std
SVC	3	**M.1.a**	**0.536220**	0.271074
		M.1.b	0.263510	0.390587
		M.2.a	0.120203	0.138596
		M.2.b	0.025974	0.044988
		R.1.a	0.581087	0.391706
		R.2	0.394412	0.103132
	5	**M.1.a**	**0.541246**	0.470426
		M.1.b	0.353514	0.333052
		M.2.a	0.220467	0.381859
		M.2.b	0.334011	0.330749
		R.1.a	0.361461	0.335237
		R.2	0.441187	0.382080
	8	M.1.a	0.743098	0.276632
		M.1.b	**0.783972**	0.152307
		M.2.a	0.628229	0.337939
		M.2.b	0.509941	0.263873
		R.1.a	0.594860	0.162840
		R.2	0.385773	0.164180
	10	M.1.a	0.265772	0.460330
		M.1.b	0.000000	0.000000
		M.2.a	**0.409449**	0.402622
		M.2.b	0.270123	0.467866
		R.1.a	0.282314	0.251124
		R.2	0.411668	0.356584
	13	M.1.a	0.665231	0.180029
		M.1.b	0.640059	0.028009
		M.2.a	0.472789	0.264564
		M.2.b	0.660249	0.000544
		R.1.a	0.660249	0.000544
		R.2	**0.769179**	0.120422

results. In fact, the levels of precision and recall for the detection of pre-ictal patterns for some of the seizure sessions, and particularly for some of the morphologic features show promise.

For the reasons outlined in the discussion, the results suffered greatly from the lack of appropriate and sufficient data-points. This lack of results, is no doubt the consequence from premature conceptions about the problem in the sense that continuous data acquisition was not possible.

There is however, no clear distinction on which feature group performs the best irrespective of the Patient, with some patients demonstrating better performances for different patterns, possibly evidencing some patient-specific pre-ictal alterations better percieved with different types of features.

It is important to refer the sucessful use of morphological features, resulting in 12 out 15 best classification performances. The use of morphological features in the seizure prediction literature is, at best, rare, and this work shows some possibility of use of these features for prediction, or at least to distinguish pre-ictal samples from inter-ictal, although the reduced volume and diminished quality of the data negatively affect the strength of such conclusions.

VII. Future Work

A possible route to explore for future works is first and foremost to gather more data. The increase the number of data points is fundamental to improve the classifiers precision and recall and in turn better identify possible pre-ictal samples.

Another possible way to improve, linked to the need to increase data volume is to ultimately improve the quality of acquired signals, with less noise and artifacts. This in turn, will surely improve the quality of the classification results, since as discussed in the previous chapters a number of seizure sessions are also corrputed by missing values.

Another more hands-on-approach to improve on these methodologies is to implement a system of alarm generators that builds on the decision function of the classifiers to detect the crossing of certain thresholds and produce automated warnings.

This implementation would in turn allow for the algorithms to be trained on the patient's data gathered from the hospital system and to use these algorithms to predict seizures based on real-time data acquisition by the wearable's system acquisition.

References

[1] A. K. Ngugi, S. M. Kariuki, C. Bottomley, I. Kleinschmidt, J. W. Sander, and C. R. Newton, "Incidence of epilepsy: A systematic review and meta-analysis," *Neurology*, vol. 77, no. 10, pp. 1005–1012, Sep. 2011.

[2] M. Winterhalder, T. Maiwald, H. Voss, R. Aschenbrenner-Scheibe, J. Timmer, and A. Schulze-Bonhage, "The seizure prediction characteristic: A general framework to assess and compare seizure prediction methods," *Epilepsy & Behavior*, vol. 4, no. 3, pp. 318–325, Jun. 2003.

[3] F. Massé, M. V. Bussel, A. Serteyn, J. Arends, and J. Penders, "Miniaturized wireless ECG monitor for real-time detection of epileptic seizures," *ACM Transactions on Embedded Computing Systems*, vol. 12, no. 4, p. 1, Jun. 2013.

[4] S. Behbahani, N. J. Dabanloo, A. M. Nasrabadi, and A. Dourado, "Prediction of epileptic seizures based on heart rate variability," *Technology and Health Care*, vol. 24, no. 6, pp. 795–810, Nov. 2016.

[5] K. Fujiwara, M. Miyajima, T. Yamakawa, E. Abe, Y. Suzuki, Y. Sawada, M. Kano, T. Maehara, K. Ohta, T. Sasai-Sakuma, T. Sasano, M. Matsuura, and E. Matsushima, "Epileptic Seizure Prediction Based on Multivariate Statistical Process Control of Heart Rate Variability Features," *IEEE Transactions on Biomedical Engineering*, vol. 63, no. 6, pp. 1321–1332, Jun. 2016.

[6] C. Varon, K. Jansen, L. Lagae, and S. Huffel, "Detection of epileptic seizures by means of morphological changes in the ECG," in *Proc. of the Computing in Cardiology Conf.*, vol. 40, Jan. 2013, pp. 863–866.

[7] P. A. Iaizzo, Ed., *Handbook of Cardiac Anatomy, Physiology, and Devices*, ser. Current clinical oncology. Totowa, N.J: Humana Press, 2005, oCLC: 990296487.

[8] R. S. Fisher, W. v. E. Boas, W. Blume, C. Elger, P. Genton, P. Lee, and J. Engel, "Epileptic Seizures and Epilepsy: Definitions Proposed by the International League Against Epilepsy (ILAE) and the International Bureau for Epilepsy (IBE)," *Epilepsia*, vol. 46, no. 4, pp. 470–472, Apr. 2005.

[9] E. Bruno, A. Biondi, and M. P. Richardson, "Pre-ictal heart rate changes: A systematic review and meta-analysis," *Seizure*, vol. 55, pp. 48–56, Feb. 2018.

[10] K. S. Eggleston, B. D. Olin, and R. S. Fisher, "Ictal tachycardia: The head–heart connection," *Seizure*, vol. 23, no. 7, pp. 496–505, Aug. 2014.

[11] K. Jansen and L. Lagae, "Cardiac changes in epilepsy," *Seizure*, vol. 19, no. 8, pp. 455–460, Oct. 2010.

[12] P. S. Hamilton, "Open Source ECG Analysis Software Documentation," *Computers in Cardiology*, vol. 2002, IEEE, pp. 101–104, 2002. [Online]. Available: http://ieeexplore.ieee.org/lpdocs/epic03/wrapper.htm?arnumber=1166717

[13] M. Malik, J. T. Bigger, A. J. Camm, R. E. Kleiger, A. Malliani, A. J. Moss, and P. J. Schwartz, "Heart rate variabilityStandards of measurement, physiological interpretation, and clinical use," *European Heart Journal*, vol. 17, no. 3, pp. 354–381, Mar. 1996.

[14] R. H. D. Townsend, "Fast Calculation of the Lomb-Scargle Periodogram Using Graphics Processing Units," *The Astrophysical Journal Supplement Series*, vol. 191, no. 2, pp. 247–253, Dec. 2010.

[15] J. T. VanderPlas, "Understanding the Lomb-Scargle Periodogram," *The Astrophysical Journal Supplement Series*, vol. 236, no. 1, p. 16, May 2018.

[16] A. Boardman, F. S. Schlindwein, A. P. Rocha, and A. Leite, "A study on the optimum order of autoregressive models for heart rate variability," *Physiological Measurement*, vol. 23, no. 2, pp. 325–336, May 2002.

[17] K. Korjus, M. N. Hebart, and R. Vicente, "An Efficient Data Partitioning to Improve Classification Performance While Keeping Parameters Interpretable," *PLOS ONE*, vol. 11, no. 8, p. e0161788, Aug. 2016.